Interpretation of the ion mass spectra in the mass range 25-35 obtained in the inner coma of Halley's comet by the HIS-sensor of the GIOTTO IMS Experiment

J. Geiss[1], K. Altwegg[1], E. Anders[1], H. Balsiger[1], W.-H. Ip[2], A. Meier[1], M. Neugebauer[3], H. Rosenbauer[2], E.G. Shelley[1,4]

[1]Physikalisches Institut, University of Bern, 3012 Bern, Switzerland
[2]Max-Planck-Institut für Aeronomie, D-3411 Katlenburg-Lindau, Federal Republic of Germany
[3]Jet Propulsion Laboratory and California Institute of Technology, Pasadena, California 91109, USA
[4]Permanent address: Lockheed Palo Alto Research Laboratory, Palo Alto, California 94304, USA

Running title:

Ion mass spectra in the inner coma of Halley's comet by GIOTTO IMS

Proofs and offprint requests to be sent to:

J. Geiss

Key word codes:

03.03.1, 03.07.1, 03.11.1, 19.06.1

Section 10:

The solar system

To be published in the Main Journal

Summary

The IMS-HIS double-focussing mass spectrometer that flew on the GIOTTO spacecraft covered the mass per charge range from 12 to 56 (AMU/e). By comparing flight data, calibration data and results of model calculations of the ion population in the inner coma, the absolute mass scale is established, and ions in the mass range 25 to 35 are identified. Ions resulting from protonation of molecules with high proton affinity are relatively abundant, enabling us to estimate relative source strengths for H_2CO, CH_3OH, HCN, and H_2S, providing for the first time a positive in situ measurement of methanol. Also upper limits for NO and some hydrocarbons are derived.

Key words: cometary atmosphere, mass spectrometry, ion spectra, molecular processes

1. Introduction

The composition of gases in the coma of comets can be studied by spectroscopy at various wave lengths of electromagnetic radiation, by mass spectrometric analysis of the neutral component, and by ion mass spectrometry. All these methods have their advantages and limitations, and it is their combination that has led to the advances in cometary chemistry that we have witnessed since the flight of spacecraft into the coma of Halley's comet.

In this paper, we use the data obtained by the HIS sensor of the IMS experiment (Balsiger et al., 1986) on the spacecraft GIOTTO during its passage through the inner coma of Halley's comet. The HIS is a double-focussing magnetic mass spectrometer with 9 channel electron multipliers (CEMs) arranged in a specially designed distributor, called an "Igel", at its exit (cf. Balsiger et al., 1986). It provides information on the mass/charge ratio, the velocity and the angles of incidence of the ions. Among the GIOTTO instruments, the capabilities of the HIS are unique for investigating the ion composition in the region between the cometopause (Gringauz et al., 1986) and the ionopause (Neubauer et al., 1986; Neubauer, 1987; Balsiger et al., 1986a) of Halley's coma.

The HIS, of course, also works in the low temperature (200-300 K) region inside the ionopause, but it is not simple to reduce the four-dimensional representation of these data (i.e. mass/charge, velocity and two angles of incidence) to a one-dimensional mass spectrum giving quantitative ion abundances, because the spectrometer response is not strictly a separable function of these four parameters. Thus, the

apparent mass/charge ratio depends somewhat on the velocity and direction of incidence. We have developed a method by which quantitative M/Q spectra are derived, using a scheme of adding CEM count rates combined with a fitting routine based on laboratory calibration data (Meier, 1988).

In contrast to previous attempts to reproduce the IMS mass spectra by ion-chemical modelling (e.g. Wegmann et al., 1987; cf. Schmidt et al., 1988), we use a model which concentrates on the ion mass range between 25 and 35 AMU/e in order to obtain better estimates of the parent molecule abundances which contribute to this ion mass range.

2. Experimental Results

The HIS sensor took data in two modes, the H- and the N-mode (Balsiger et al., 1986; Meier, 1988). Results obtained in the H-mode for the mass range 12 to 35 at nine distances from the nucleus are shown in Figs. 1 and 2. Each spectrum represents the data of one spin period, corresponding to a traversal of 273 km. The distances from the nucleus given in the figures are determined at the centers of the respective spin periods. The HIS instrument scans the voltage of the energy analyzer in 64 steps, covering the energy range appropriate for rammed cold ions with mass/charge 12 to 56. In the innermost part of the coma a countrate vs. measurement step plot represents a mass spectrum, because all cold ions have the same velocity in the instrument frame of reference, i.e. the ram velocity (68.4 km/s). The H- and N-mode are different in so far that in the H-mode all masses with the same

angle and velocity are measured by the same CEM, whereas in the N-mode different masses are deflected to different CEMs. Hence the H-mode is well suited to get full survey mass spectra (by plotting countrates vs. measurement step). However, the assignment of mass in the measurement step/CEM-matrix is dependent on ion speed, temperature and angle, and the detailed response of the matrix bins to each ion beam had to be carefully calibrated. Thus, for the purposes of this paper, we use the H-mode to give an overview of the spectra as a function of distance from the nucleus. The N-mode data are then used to derive relative ion abundances based on the calibrated response function.

Up to about mass 20, the identification of the ionic masses does not pose a problem, thus there is no uncertainty in the mass scale given in Fig. 1. This is supported by the fact that the calibration data predict the position of H_3O^+ where the highest ion peak is actually found. From this part of the spectrum, we can determine velocity and angle of incidence of the ions. If we then assume that the velocities and the flow directions are the same for all masses, we can assign an accurate mass scale to the higher masses as well. In Fig. 2, we give the H-mode spectra thus obtained for the ions in the range M/Q = 25-35.

The data displayed in Figs. 1 and 2 divide naturally into three spatial regions as can be recognized in the patterns of the spectra.

I. 1215 km - 3289 km. This region lies well inside the contact surface (Neubauer et al., 1986; Neubauer, 1987; Balsiger et al., 1986a). Here the counts are fairly evenly distributed in azimuth indicating that the flow direction coincides with the spin axis. The

ion temperature is less than 500 K. The M/Q patterns of the five spectra are fairly similar and indicate a good tuning of the instrument and a good mass resolution for the regular flow velocity encountered here.

II. 4365 - 6554 km. This region lies mainly outside the contact surface (at 4660 km, Neubauer, 1987). The counts are unevenly distributed over azimuth in this region, indicating a flow with a velocity component coming from the solar direction. This is consistent with expectation since bulk flow of the ions should follow roughly the contours of the contact surface. The 4365 km spectrum contains data from inside the contact surface. It was here that the HERS sensor detected hot cometary ions which may be due to the double charge-exchange mechanism (Goldstein et al., 1987; Eviatar et al., 1989). The flow conditions and distribution functions in region II are significantly different from those in region I. The poor mass definition and resolution shown for the region II spectra in Figs. 1 and 2 results from the fact that they were generated using the flow conditions prevailing in region I.

III. 9814 km. This spectrum is typical of the region outside ~7500 km. The azimuthal anisotropy is still observed, compatible with the expected flow pattern around the contact surface. The spectrum is similar to those in region I, with the exception of the strong count rate at M/Q = 32. The latter may result from a change in chemical composition with distance (i.e. there is a slow build-up of S^+; cf. section 4).

3. Interpretation of the spectra

This paper is concerned primarily with the ion mass range 25 to 35 AMU/e (Fig. 2) focussing on region I, i.e. the low temperature gas inside the contact surface. Here, photodissociation, photoionization, ion-molecule reactions, and dissociative recombination dominate the chemistry. The dominance of water vapor in the neutral gas together with its high proton affinity (PA) results in H_3O^+ being by far the most abundant ion. Thus, this ion governs the direction that the ion-molecule reactions take (Aikin, 1974). As a consequence, the PA of the molecules or radicals in the inner coma (Table 1) is the most important chemical parameter (Huntress, 1977), determining what the main ionized species are for a particular parent molecule.

Molecules (M) having a higher PA than water (cf. Table 1) react readily with H_3O^+ abstracting a proton:

$$H_3O^+ + M \rightarrow H_2O + MH^+ \ . \qquad (k1)$$

Consequently, the resulting MH^+ ions (Table 2, column 3) are very abundant relative to their parent molecules. For molecules containing H, C, and O, reactions with H_3O^+ have the effect of transforming a molecular mass spectrum dominated by even numbers into an ion mass spectrum dominated by odd numbers.

On the other hand, ions M^+ produced by simple photoionization (emission of an electron) from a molecule having a PA lower than water fall into two categories. If they react with water (e.g. CO^+, cf. Table 1)

$$M^+ + H_2O \rightarrow \text{products} \qquad (k2)$$

they will have a low abundance (Table 2, column 5). If they do not react with water (e.g. NO^+; cf. Table 1), they will have a rather long lifetime, governed in most cases by dissociative recombination, and thus they will accumulate towards a relatively high abundance (Table 2, column 4).

While these simple systematics are qualitatively valid, ion-molecule reactions with species other than the most abundant H_2O and H_3O^+ must be taken into account for a quantitative analysis. For this purpose, we have developed a numerical method which is simple, yet adequate for treating the radial evolution of ion abundances in the inner coma (Appendix A). The 21 neutral and 40 ion species listed in Table 3 were included in the calculations for the present paper. The parent molecules selected fall into three categories: (1) Those which could reasonably be expected and are essential to obtain an adequate fit to the data (e.g. H_2O, CO), (2) those which have been previously reported but cannot be positively confirmed or excluded by the data (e.g. N_2), and (3) theoretically possible molecules for which the data provide abundances (H_2CO, CH_3OH, NCN, H_2S) or meaningful upper limits (e.g. NO, hydrocarbons). Photodissociation and photoionization of all neutral species, dissociative recombination of the ions, and about 280 ion-molecule reactions were taken into account. Information on the rate constants that were used is given in Appendix B. While the expansion velocity could be introduced into the program as a function of radial distance, for the purpose of this paper, which deals with the coma inside the contact surface, the expansion velocity was assumed to be a constant 900 m/s (cf. Lämmerzahl et al., 1987). The program allows for molecular point sources (near the nucleus) and for extended sources. We have used a point source for H_2O with a strength

corresponding to a H_2O density of 5×10^7 cm^{-3} at 1000 km from the nucleus (Krankowsky et al., 1986). Strengths of point sources or extended sources for the other neutral species given in Table 3 could be freely chosen. Many numerical integrations varying these source strengths were carried out in order to study the influence of individual components and combinations of components.

As discussed above, the mass scale can be influenced by various parameters including angle of incidence and ion speed. The results can be summarized as follows: With the mass scale given in Fig. 2, we find a reasonable set of molecular abundances that can reproduce the observed ion mass spectra in the mass per charge range 25 to 35. We have not been able to find an alternative mass assignment that could do this. For instance, a shift of all peaks by one unit to higher M/Q values could not be ruled out absolutely by the calibration data alone. However, we would have no explanation for a high abundance at M/Q = 34 along with a low abundance at M/Q = 35; e.g. H_2S would produce the opposite effect. Also, a relatively high flux of M/Q = 29 ions could not be explained: HCO^+ has to be lower than CO^+, and $C_2H_5^+$ or N_2H^+ react with H_2O with high rate constants.

A shift of all peaks by one unit to lower M/Q values would be difficult to reconcile with the calibration data. Moreover, it would again be difficult to find a chemical interpretation (cf. Table 2). For instance, it would be hard to explain the high abundance at M/Q = 30 that results with this mass scale.

On the other hand, the mass scale given in Fig. 2 results in relative abundance peaks inside the contact surface at the four mass

numbers corresponding to the products of H_3O^+ listed in column 3 of Table 2. In other words, the pattern in the mass range 25 to 35 finds a natural explanation. A careful comparison of this mass scale with the calibration data implies that the average arrival direction of the ions was ~0.3 degrees away from the optical axis of the entrance deflector of the HIS sensor and that the ions had an average radial speed of 900 m/s. These parameters also fit the lower mass ions given in Fig. 1, for which the mass assignment is not in question.

With the adopted mass scale, we interpret the spectra obtained between 1215 km and 3289 km as follows:

1. Because of their high proton affinity, H_2CO and CH_3OH dominate the mass range 25 to 35, being the parent molecules of the two most abundant ions (CH_3O^+ and $CH_3OH_2^+$).

2. The minimal ion abundances at masses 27, 29, and 34 are consistent with prediction. All ions listed in Tables 2 and 3 with these masses ($C_2H_3^+$, HCN^+, $C_2H_5^+$, N_2H^+, HCO^+, H_2S^+), and also $H_2O_2^+$, react with water.

3. The peak height at mass 28 is consistent with the HCN/H_2O abundance ratio of 0.001 derived by Schloerb et al. (1987) from radio frequency observations. CO^+ also contributes to the mass 28 peak but is not dominant.

4. The hydrocarbons C_2H_n are difficult to determine from the ion spectra. At this time, only upper limits can be given. The small peak at mass 26, if real, would be due to $C_2H_2^+$, rather than CN^+, since the latter is readily destroyed by water (Tables 1 and 2).

For the purpose of deriving molecular abundances, we have computed ion mass spectra as a function of distance from the nucleus, varying the proportions of the assumed parent molecules to optimize the fit. In Fig. 3, we compare such a computed spectrum, based on the abundances indicated, with the observed spectra at two radial distances straddling that of the computation. It is evident that the fit is quite reasonable. The sensitivity of the fit to variations in the parent molecule source strengths was investigated in order to establish ranges or limits.

As noted in Fig. 3, contributions from extended sources were assumed for some molecules. For these we assume an exponential depletion length of 10^4 km, originating at the nucleus. Such extended sources are indicated by the comprehensive CN-observations of A'Hearn et al. (1986) and Hoban et al. (1988), as well as by the mass spectrometer results for neutral CO (Eberhardt et al., 1987). While the need to include both point and extended sources is clearly indicated, both from the previous work and our data, the distance between the two experimental spectra given in Fig. 3 is too small for arriving at a reliable quantitative separation between them. For this, a complete investigation of the radial evolution of each ion in question would be required.

We emphasize that the molecular abundances shown in Fig. 3 are not unique in giving a reasonable agreement between theoretical and experimental spectra, considering the uncertainties in the experimental data and in the reaction rate constants. Definite abundance estimates can be obtained, however, for molecules having high PAs, because the ions resulting from their protonation dominate the mass

spectra. This is evident from Table 4 where the relative contributions to some relevant mass numbers are listed.

4. Molecular Abundances

Below, we give abundance estimates derived from a comparison of the results of the model calculations with the measured spectra in region I. We do not distinguish between point sources and extended sources for most molecular species. Some of the abundances might be improved by applying a more refined fitting programme to the data and by comparing experimental and theoretical ion abundances over the whole length of the trajectory inside the contact surface. However, we are confident that the resultant improvements would not materially alter the conclusions, and thus the added complexity of the modeling is not justified for the purposes of this paper.

Ammonia. NH_3 can be estimated from the NH_4^+/H_3O^+ ratio (Ip, 1986). Allen et al. (1987), using IMS data, applied this method to derive a NH_3/H_2O abundance ratio of .01 to .02; however, they neglected reactions of H_3O^+ with molecules heavier than water. Ip et al. (1990) pointed out that even relatively rare HCN influences the ammonia abundance thus derived. Now that we find a few to several percent of molecules with higher PA than water, we obtain a reduction of H_3O^+, which in turn somewhat reduces the estimate on the NH_3/H_2O ratio. The question of whether or not the ratio thus obtained is compatible with the NH_3/H_2O value of 0.003 derived from the NH_2 emission (Wyckoff et al., 1988) will be discussed in a separate paper.

Formaldehyde. The mass 31 ion rate falls off less rapidly than R^{-1} between 1215 km and 9814 km (cf. Fig. 2) in spite of the relatively short photo lifetime of H_2CO (cf. Table 2). From this, we derive a H_2CO source which is at least partly extended with an integrated strength (relative to water) of about one percent at 1500 km, rising to a few percent at the ionopause. The mass spectra measured in region II suggest that the source extends even farther out. Our results are in agreement with data obtained by other instruments. H_2CO has been found with the IKS infrared spectrometer on the VEGA 1 spacecraft (Combes et al., 1988; Mumma and Reuter, 1989). Polymeric formaldehyde has been inferred from the spectra obtained by the ion energy spectrometer PICCA onboard the GIOTTO spacecraft (Mitchell et al, 1987; Huebner, 1987) . Krankowsky (1990) found the formaldehyde molecule with the GIOTTO NMS mass spectrometer. He estimated a H_2CO abundance relative to water of 4.5 percent, including a contribution from an extended source.

Methanol. The peak at mass 33 could be protonated methanol or hydrazine. Stief and deCarlo (1965) and Delsemme (1975) have proposed that the 3360 Angström emission observed in comets is due to a NH radical, the precursor of which is hydrazine. Under the thermodynamic conditions in the solar nebula or the proposed sub-nebula (Fegley and Prinn, 1988), N_2H_4 would not be produced in significant amounts. Calculations show that the equilibrium ratio N_2H_4/N_2 for these two sites is only 2×10^{-38} and 3×10^{-29} at 300 K or 4×10^{-20} and 3×10^{-11} at 1500 K. The equilibrium ratio CH_3OH/CO is higher, especially in a sub-nebula environment. Also, there has been no mentioning of hydrazine production in interstellar clouds, whereas some ammonia and methanol are produced according to ion molecule reaction calculations (cf. Prasad

and Huntress, 1980; Leung et al., 1984). Moreover, if we wanted to identify the mass 33 peak with $N_2H_5^+$, we would have to postulate $N_2H_4/NH_3 \geq 1$ which seems implausible. Thus, we propose that the mass 33 peak is essentially due to $CH_3OH_2^+$ which leads to an estimate of the methanol/ water ratio of .003 to .015. This is the first in situ measurement of CH_3OH in a comet. However, methanol has also recently been found in comet Austin by millimeter observations (Colom et al., 1990).

Nitrous Oxide. The count rate at mass 30 places an upper limit of .005 on NO/H_2O. NO is usually not mentioned among possible cometary constituents. Since, however, theory indicates that NO is produced in dense interstellar clouds (Prasad and Huntress, 1980), it may be well to mention this NO abundance limit for Halley's coma.

Hydrogen Cyanide. The peak at mass 28 is probably mainly due to H_2CN^+. Although CO is the second most abundant molecule in Halley's coma (Eberhardt et al., 1987), the contribution of CO^+ is minor, because this ion reacts readily with water (cf. Tables 1, 2, and 4). If we assume that also C_2H_4 does not contribute very much, then we have enough H_2CN^+ to account for the $HCN/H_2O \sim .001$ abundance ratio derived from radio frequency observations (Schloerb et al., 1987) or from the CN emission (A'Hearn et al., 1986). Our estimate for the HCN abundance is higher than the one given by Ip et al. (1990).

Hydrocarbons. Since C_2H_6, C_2H_4, and C_2H_2 have PAs lower than water, they do not form ions with prominent abundances. However, the count rates at masses 25 and 26 indicate that some hydrocarbon ions are present in the mass range considered. While a careful analysis of

the abundances - particularly at even mass number - might produce some definite hydrocarbon estimates, we simply mention that as a result of our present modelling effort the sum of the abundances of acetylene and ethylene are at most one or two percent relative to water.

H_2S and S. The inclusion of S, H_2S and related ions was intended to allow for studying their contribution in the mass range considered. We defer a more complete discussion of the sulfur containing species to a later publication and discuss here only the abundance of H_2S, which has just been detected in comet Austin by millimeter observation (Colom et al., 1990). For comet Halley's coma, Marconi et al. (1990) derived a *lower* limit of 0.5 percent for the H_2S/H_2O ratio. However, their conclusion is based on a dissociation time for H_2S of ∿300 sec, which we consider to be erroneous for two reasons: (1) The photolysis of H_2S leads to SH which in turn dissociates in 118 sec (0.9 AU; Kim and A'Hearn, 1990) to give S. From atomic sulfur, S^+ is produced at a relatively high rate (Table B1). Thus, not only H_3S but also S^+ carries significant information on the occurrence of H_2S. Our model calculations clearly show that H_2S with a half percent abundance and a lifetime of only ∿300 sec would lead to a much higher ion abundance at mass 32 than we actually observe (cf. Fig. 3). (2) Using the cross section data given by Lee et al. (1967), Kim and A'Hearn (1990) have derived a photodissociation time for H_2S of 3200 sec (0.9 AU), a result we have confirmed. With this longer dissociation time, we have consistency between the masses 35 and 32 in the ion spectra and obtain a H_2S source strength (point source and/or extended source) of 0.001 to 0.004 relative to H_2O.

There is a significant change in the appearance of ion mass spectra in region II relative to region I (Figs. 1 and 2). As pointed out in Section 2, the distribution functions of the ions have changed significantly from the quiet flow encountered in region I. This makes it difficult to identify changes in ion abundances with the methods used in this paper, since these methods are based on the assumption of quiet flow conditions appropriate to region I.

While the perturbations in the spectra observed in the mass range 16-20 in region II have again disappeared in region III (Fig. 1), the high count rate at M/Q = 32 remains (Fig. 2). A slow build-up of M/Q = 32 actually begins between 2000 and 3000 km. Thus, this general increase in M/Q = 32 with increasing distance could be due to the S^+ ion. However, quantitative interpretation of the spectra in regions II and III needs further analyses, which we leave to future publications.

5. Discussion

The ions CH_3O^+ and $CH_3OH_2^+$ are derived from formaldehyde and methanol, respectively. Judging from ion-molecule reaction systematics, it seems improbable that heavier gaseous aldehydes, ketones or alcohols contribute significantly to these ions. Thus, we propose that both H_2CO and CH_3OH are present in the gas phase with the relative abundances indicated in Section 4. This observation neither precludes nor supports the possibility that H_2CO and/or CH_3OH are present in some polimerized form in the solid (Vanysek and Wikramasinghe, 1975; Huebner, 1987; Mitchell et al., 1987). The radial decrease of CH_3O^+ is less

than expected for a point source, indicating that H_2CO is released from grains over times of the order of hours.

The analysis offered here underlines that carbon in Halley's comet exists largely in oxidized form - at least the portion of it that is released into the gas phase within the first one or two hours.

Krankowsky et al. (1986a) have shown that the dominating peaks in the 40-50 mass region occur at M/Q = 45 and M/Q = 47, and they identify them as HCS^+ and H_3CS^+, respectively. We note that protonized *acetaldehyde* (CH_3CHO) and *ethylalcohol* (C_2H_5OH) may significantly contribute to these mass peaks.

Acknowledgements

The authors wish to acknowledge advice and comments by Drs. M.F. A'Hearn, M. Coplan, E.E. Ferguson, E. Herbst, and E. Kopp. They thank Mrs. Graziella Troxler for preparing the manuscript. This work was supported by the Swiss National Science Foundation. The research at JPL was done under a contract between the California Institute of Technology and NASA under the sponsorship of the Magnetospheric Physics program. The research at Lockheed was supported by NASA through contract NASW-4336 and Lockheed Independent Research. This paper was completed while E. Shelley worked as a Visiting Professor at the University of Bern, supported by the Bern Government, and while J. Geiss was a Visitor at the Institute of Science and Technology and the Space Physics Group of the University of Maryland in College Park and a National Academy/National Research Council Senior Associate at the NASA Goddard Space Flight Center, Greenbelt, MD.

Appendix A

The chemistry in the ionosphere - the region well inside the contact surface - of Halley's comet is dominated by photodissociation, photoionization, ion-molecule reactions, and dissociative recombination. Since these reactions and in particular the ion-molecule reactions connect a great variety of species in a rather non-systematic way, a large matrix of non-linear differential equations results.

The ionosphere is characterized by a steady expansion velocity of ∿0.9 km/s which is roughly equal for ions and neutrals (Krankowsky et al., 1986; Lämmerzahl et al., 1987) and by low kinetic temperatures (200-300 K; Balsiger et al., 1986a). Thus, the rate constants for ion- molecule reactions measured in the laboratory can be used.

We found reactions between neutrals (molecules or radicals) to be of minor importance for the species considered here; thus, we have neglected this type of reaction. In fact, the most important change in neutral abundances comes from photodissociation (and ionization) and this has been taken into account.

The ion abundances originally obtained from photoionization are thoroughly changed by ion-molecule reactions. On the other hand, for the neutral partners the relative importance of these ractions is small because of the relatively low abundance of the ions. Thus, we have neglected the changes in neutral abundances due to ion-molecule reactions. The types of reactions included in our model are given in the following equations (reactants or products for which the changes due to the reaction are taken into account in our calculations are underlinded):

$$\underline{A} + h\nu \rightarrow \underline{B} + \underline{C} + \ldots\ldots \quad (1)$$

$$\underline{A} + h\nu \rightarrow \underline{B^+} + \underline{e^-} + \underline{C} + \ldots\ldots \quad (2)$$

$$A + \underline{B^+} \rightarrow C + \underline{D^+} \quad (3)$$

$$\underline{B^+} + \underline{e^-} \rightarrow C + D \quad (4)$$

It is seen that with the simplifications introduced here, the first three types of equations are linear.

The set of differential equations corresponding to the reaction equations (1) to (4) is solved by stepwise integration over r, the distance from the nucleus. The relation between time t and r is given by the expansion velocity v(r) which was taken to be constant at 900 m/s. A backward integration scheme was chosen for the destruction terms, but not for the production terms which were treated according to the forward method. In this way, the differential equations are decoupled, and a matrix conversion procedure is avoided.

The reaction rates of equations (1) to (4) form one-, two- or three-dimensional arrays of real numbers. Since many elements in these arrays are empty, we have the code first establish arrays with integers 0 or 1 depending on whether the corresponding element in the real number array vanishes or not. These integer number arrays are interrogated at each integration step. Empty elements of the arrays are skipped; thus, a large number of useless real number multiplications are avoided. These simplifications led to a program which can be used in an interactive mode on a modest PC and the numbers of species and reactions considered can be easily changed.

Appendix B

A large number of photodissociation, photoionization, ion-molecule reaction and recombination rates are used in this investigation. However, only a part of these rates have a major influence on the relative abundances of ions and molecules discussed in Section 4. Therefore, we present in this paper the numerical values only for these important rate constants. References are given for the others.

Photodissociation and Photoionization

Rates corresponding to quiet solar conditions at 0.9 AU were used. Photoionization is of major importance for molecules that do not react with H_3O^+. The rate constants for the ions listed in column 4 of Table 2 are given in Table B1.

Ion-Molcule Reactions

Rate constants were taken from the following compilations: Anicich and Huntress (1986), Allen et al. (1987), Prasad and Huntress (1980), Giguere and Huebner (1978), Huebner and Giguere (1980). The most important rate constants, i.e. those for reactions with H_2O and H_3O^+, are given in Table 1. Atomic sulphur was introduced as a possible source of S^+ ions (cf. text); however, reactions of ions with S were not included.

Dissociative Recombination

Dissociative recombination is usually the dominant destruction mechanism for ions that do not react with water. The corresponding rates, evaluated at 273 K, are given in Table B2. Rates not found in the literature were estimated.

References

Adams, N.G., Smith, D.: 1988, Chemical Phys. Lett. 144, 11

A'Hearn, M.F., Hoban, S., Birch, P.V., Bowers, C., Martin, R., Klinglesmith, D.A.: 1986, Nature 324 649

Aikin, A.C.: 1974, Astrophys. J. 193, 263

Allen, M., Delitsky, M., Huntress, W.T., Yung, Y., Ip, W.-I., Schwenn, R., Rosenbauer, H., Shelley, E., Balsiger, H., Geiss, J.: 1987, Astron. Astrophys. 187, 502

Anicich, V.G. and Huntress, W.T.: 1986, Astrophys. J. Suppl. 62, 553

Ausloos, P.: 1974, Interaction Between Ions and Molecules, Plenum Press, New York and London, p. 415

Balsiger, H., Geiss, J., Young, D.T., Rosenbauer, H., Schwenn, R., Ip, W.-H., Ungstrup, E., Neugebauer, M., Goldstein, R., Goldstein, B.E., Huntress, W.T., Shelley, E.G., Sharp, R.D., Johnson, R.G., Lazarus, A.J., Bridge, H.S.: 1986, ESA-SP 169, 93

Balsiger, H., Altwegg, K., Bühler, F., Geiss, J., Ghielmetti, A.G., Goldstein, B.E., Goldstein, R., Huntress, W.T., Ip, W.-H., Lazarus, A.J., Meier, A., Neugebauer, M., Rettenmund, U., Rosenbauer, H., Schwenn, R., Sharp, R.D., Shelley, E.G., Ungstrup, E., Young, D.T.: 1986a, Nature 321, 330

Colom, P., Despoir, D., Bockelee-Morvan, D., Crovisier, J., Paubert, G.: 1990, to be published in the Proceedings of the Workshop "Observations of Recent Comets", Albuquerque, New Mexico, USA, June 1990

Combes, M., Moroz, V.I., Crovisier, J., Encrenaz, T., Bibring, J.-P., Grigoriev, A.V., Sanko, N.F., Coron, N., Crifo, J.F., Gispert, R., Bockelée-Morvan, D., Nikolsky, Yu. V., Krasnopolsky, V.A., Owen, T., Emerich, C., Lamarre, J.M., Rocard, F.: 1988, The 2.5 to 12 μm spectrum of comet Halley from the IKS-VEGA experiment, Icarus 76, 404

Delsemme, A.H.: 1975, Icarus 24, 95

Eberhardt, P., Krankowsky, D., Schulte, W., Dolder, U., Lämmerzahl, P., Berthelier, J.J., Woweries, J., Stubbemann, U., Hodges, R.R., Hoffman, J.H., Illiano, J.M.: 1987a, Astron. Astrophys. 187, 481

Eviatar, A., Goldstein, R., Young, D.T., Balsiger, H., Rosenbauer, H., Fuselier, S.A.: 1989, Astrophys. J. 339, 545

Fegley, B. Jr., Prinn, R.G.: 1988, in The Formation and Evolution of Planetary Systems, Eds. H.A. Weaver, F. Paresce, L. Danly, Cambridge U. Press, Cambridge

Giguere, P.T., Huebner, W.F.: 1978, Astrophys. J. 223, 638

Goldstein, R., Young, D.T., Balsiger, H., Bühler, F., Goldstein, B.E., Neugebauer, M., Rosenbauer, H., Schwenn, R., Shelley, E.G.: 1987, Astron. Astrophys. 187, 220

Gringauz, K.I., Gombosi, T.I., Tâtrallyay, M., Verigin, M.I., Remizov, A.P., Richter, A.K., Apàthy, I., Szemerey, I., Dyachkov, A.V., Balakina, O.V., Nagy, A.F.: 1986, Geophys. Res. Lett. 7, 613

Heppner, R.A., Walls, F.L., Armstrong, W.T., Dunn, G.H.: 1976, Phys. Rev. A, 13, 1000

Hoban, S., Samarasinha, N.H., A'Hearn, M.F., Klinglesmith, D.A.: 1988, Astron. Astrophys. 195, 331

Huebner, W.F.: 1987, Science 237, 628

Huebner, W.F., Giguere, P.T.: 1980, Astrophys. J. 238, 753

Huntress, W.T.: 1977, Astrophys. J. Suppl. 33, 495

Ip, W.-I., 1986: Adv. Space Res. 5, 233

Ip, W.-I., Balsiger, H., Geiss, J., Goldstein, B.E., Kettmann, G., Lazarus, A.J., Meier, A., Rosenbauer, H., Schwenn, R., Shelley, E.G.: 1990, Giotto IMS Measurements of the Production Rate of Hydrogen Cyanide in the Coma of Comet Halley, Ann. Geophys., in press

Kim, S.J., A'Hearn, M.F.: 1990, unpublished

Krankowsky, D., Lämmerzahl, P., Herrwerth, I, Woweries, J., Eberhardt, P., Dolder, U., Herrmann, U., Schulte, W., Berthelier, J.J., Illiano, J.M., Hodges, R.R., Hoffman, J.H.: 1986, Nature 321, 326

Krankowsky, D., Eberhardt, P., Berthelier, J.J., Dolder, U., Hodges, R.R., Hoffman, J.H., Illiano, J.M., Lämmerzahl, P., Schulte, W., Stubbemann, U., Woweries, J.: 1986a, Proc. 20th ESLAB Symposium on the Exploration of Halley's Comet, Heidelberg, 27-31 October 1986, ESA SP-250, Vol. I, 381

Krankowsky, D.: 1990, The composition of comets, in Comets in the Post-Halley Era, Eds. R.L. Newburn, J. Rahe, Kluwer Academic Publishers, Dordrecht, p. 1

Lämmerzahl, P., Krankowsky, D., Hodges, R.R., Stubbemann, U., Woweries, J., Herrwerth, I., Berthelier, J.J., Illiano, J.M., Eberhardt, P., Dolder, U., Schulte, W., Hoffman, J.H.: 1987, Astron. Astrophys. 187, 169

Lee, L.C., Wang, X., Suto, M.: 1987, J. Chem. Phys. 86, 4353

Levine, J.S.: 1985, The Photochemistry of Atmospheres, Academic Press, Orlando, Appendix I

Leung, Ch. M., Herbst, E., Huebner, W.F.: 1984, Astrophys. J. Suppl. Ser. 56, 231

Marconi, M.L., Mendis, D.A., Korth, A., Lin, R.P., Mitchell, D.L., Rème, H.: 1990, Astrophys. J. 352, L 17

McGowan, J. Wm., Mitchell, J.B.A.: 1984, Electron-Molecule Interactions and Their Applications, Vol. 2, ed. L.G. Christophorou, Academic Press, Orlando, p. 65

Meier, A.: 1988, Ph.D. Thesis, University of Bern

Mitchell, D.L., Lin, R.P., Anderson, K.A., Carlson, C.W., Curtis, D.W., Korth, A., Rème, H., Sauvaud, J.A., d'Uston, C., Mendis, D.A.: 1987, Science, 237

Mumma, M.J., Reuter, D.: 1989, Astrophys. J. 344, 940

Neubauer, F.M., Glassmeier, K.H., Pohl, M., Raeder, J., Acuna, M.H., Burlaga, L.F., Ness, N.F., Musmann, G., Mariani, F., Wallis, M.K., Ungstrup, E., Schmidt, H.U.: 1986, Nature 321, 352

Neubauer, F.M.: 1987, Astron. Astrophys. 187, 73

Prasad, S.S., Huntress, W.T.: 1980, Astrophys. J. suppl. 43, 1

Radzig, A.A., Smirnow, B.M.: 1980, Reference Data on Atoms, Molecules, and Ions, Springer, Berlin, p. 438

Schloerb, F.P., Kinzel, W.M., Swade, D.A., Irvine, W.M.: 1987, Astron. Astrophys. 187, 475

Schmidt, H.U., Wegmann, R., Huebner, W.F., Boice, D.C.: 1988, Computer Physics Communications 49, North-Holland, Amsterdam, 17

Stief, L.J., deCarlo, V.J.: 1965, Nature 4974, 889

Vanysek, V., Wickramasinghe, N.C.: 1975, Astrophys. Space Sci. 33, L19

Wegmann, R., Schmidt, H.U., Huebner, W.F., Boice, D.C.: 1987, Astron. Astrophys. 187, 339

Wyckoff, S., Tegler, S., Wehinger, P., Spinrad, H., Belton, M.J.S.: 1988, Astrophys. J. 325, 927

Figure Captions

Fig. 1. Nine mass spectra in the AMU/e range 12 to 24 obtained in the H-mode of the HIS sensor. Distances to the nucleus are indicated. The spectra obtained in the three regions of the inner coma described in the text are distinguished by solid lines (region I), dashed lines (region II), and short dashed lines (region III).

Fig. 2. The same spectra as in Fig. 1 for the AMU/e range 25 to 35.

Fig. 3. Relative ion densities derived from the N-mode data at 1485 km (diamonds and bold dashed line) and 1950 km (triangles and fine dashed line) from the nucleus. These experimental spectra are compared with a model ion spectrum (crosses and solid line) which was calculated at the intermediate distance of 1717 km with the molecular abundances shown in the insert. S_p indicates a point source and S_E indicates an extended source ($R^{-2}e^{-R/10000}$).

Table 1. Proton affinities (PA) and rate constants k_1, k_2

	PA (eV)	k_1		PA (eV)	k_2
NH_3	8.9	2.2	C_2H_4 [3]	7.1	< .001
			C_2H_6	6.9	2.95
C_2H_5OH	8.16	2.8	C_2H_2	6.7	.22
CH_3CHO	8.07	3.6	HCO	6.6	3.0
CH_3OH	7.9	2.8	OH	6.18	2.89
N_2H_4	7.9 [1]		CO	6.15	2.6
HCOOH	7.81	2.7	CH_4	5.7	2.5
H_2CO	7.5	3.4 [2]	CO_2	5.68	2.2
HCN	7.43	4.0	NO	5.5	--
H_2S	7.4	1.9	CH_3	5.4	≤ .01
			N_2	5.1	2.5
			CN	∿5	3.2
H_2O	7.20		O_2	4.38	< .001
			H_2	4.38	7.3

Proton Affinities from Radzig and Smirnow (1980) and Ausloos (1974)

Rate constants k_1 and k_2, defined in the text, in 10^{-9} cm^3 s^{-1} from Anicich and Huntress (1986)

[1] from dissociation constant

[2] the reverse reaction has a rate of $\sim.23\times10^{-9}$ cm^3 s^{-1}

[3] $k_1 = .06\times10^{-9}$ cm^3 s^{-1}

Table 2. Inner coma: Ions in the 25-35 mass range[1]

Parent Molecules	Photo lifetime[2] (s)	Ions in Relation to Abundances of Parent Molecules: Major Ions Produced by H_3O^+	Long-lived[3] Ions Produced by Photons	Minor Ions Destroyed by H_2O
H_2S (34)	3.2×10^3	H_3S^+ (35)		H_2S^+ (34) HS^+ (33)
CH_3OH (32)	3.1×10^3	$CH_3OH_2^+$ (33)		CH_3OH^+ (32)
S (32)	9×10^5		S^+ (32)	
H_2CO (30)	2.9×10^3	CH_3O^+ (31)		H_2CO^+ (30)
NO (30)	2.4×10^5		NO^+ (30)	
C_2H_6 (30)	4.9×10^4			$C_2H_6^+$ (30) $C_2H_7^+$ (31)
C_2H_4 (28)	1.9×10^4		$C_2H_4^+$ (28)[6]	$C_2H_5^+$ (29)[6]
CO (28)	1.3×10^6			CO^+ (28) HCO^+ (29)
N_2 (28)	8.1×10^5			N_2^+ (28) N_2H^+ (29)
HCN (27)	7.7×10^5	H_2CN^+ (28)		HCN^+ (27) CN^+ (26)
C_2H_2 (26)	2.6×10^4		C_2H^+ (25)[4] $C_2H_2^+$ (26)[5,6]	$C_2H_3^+$ (27)[6]

1] Mass numbers in parenthesis

2] 0.9 AU; data from Levine (1985); Kim and A'Hearn (1990)

3] Not destroyed by H_2O

4] Possibly also produced by He^+ near and outside the contact surface

5] Slowly reacting with H_2O (cf. Table 1)

6] Various hydrocarbons may contribute to this ion

Table 3. Molecules and Ions Included in the Coma Model Calculations

Molecules

H, H_2, O, OH, H_2O

C, CH_4, C_2H_2, C_2H_4, C_2H_6

N, NH_3, HCN, N_2, NO

CO, H_2CO, CH_3OH, CO_2

S, H_2S

Ions

H^+, H_2^+, O^+, OH^+, H_2O^+, H_3O^+

C^+, CH_2^+, CH_3^+, CH_4^+, CH_5^+

C_2H^+, $C_2H_2^+$, $C_2H_3^+$, $C_2H_4^+$, $C_2H_5^+$, $C_2H_6^+$, $C_2H_7^+$

N^+, NH^+, NH_2^+, NH_3^+, NH_4^+

HCN^+, H_2CN^+, N_2^+, N_2H^+, NO^+

CO^+, HCO^+, H_2CO^+, H_3CO^+, CH_3OH^+, $CH_3OH_2^+$

CO_2^+, HCO_2^+

S^+, HS^+, H_2S^+, H_3S^+

Table 4. Relative contributions of ions to some important mass numbers. These percentages refer to the theoretical ion mass spectrum shown in Fig. 3.

Mass-28	Mass-30	Mass-31	Mass-32	Mass-33
H_2CN^+ = 69%	NO^+ = 87%	H_3CO^+ = 100%	CH_3OH^+ = 62%	$CH_3OH_2^+$ = 99%
CO^+ = 20%	H_2CO^+ = 12%		S^+ = 38%	SH^+ = 1%
$C_2H_4^+$ = 11%	$C_2H_6^+$ = 1%			

Table B1. Photoionization rates at 0.9 AU

Molecule	Ion	Rate 10^{-7} s^{-1}
H_2O	H_2O^+	4.1
CO	CO^+	3.8
NO	NO^+	16.0
C_2H_2	$C_2H_2^+$	9.6
C_2H_2	C_2H^+	.9
C_2H_4	$C_2H_4^+$	7.2
C_2H_4	$C_2H_2^+$	2.5
S	S^+	12.0

Data are for quiet solar condition (Levine, 1985; Appendix I) at 0.9 AU

Table B2. Dissociative recombination rates with electrons at 273 K

Ion	k (10^{-7} cm^3 s^{-1})	
NH_4^+	15.9	(a)
H_3O^+	10	(a,b)
C_2H^+	5.7	(a)
$C_2H_2^+$	5.7	(a)
$C_2H_4^+$	10	(d)
H_2CN^+	3.5	(c)
NO^+	4.6	(a)
CH_3O^+	10	(d)
$CH_3OH_2^+$	8.8	(c)
H_3S^+	3.7	(c)

(a) McGowan and Mitchell (1984)
(b) Heppner et al. (1976)
(c) Adams and Smith (1988)
(d) estimate

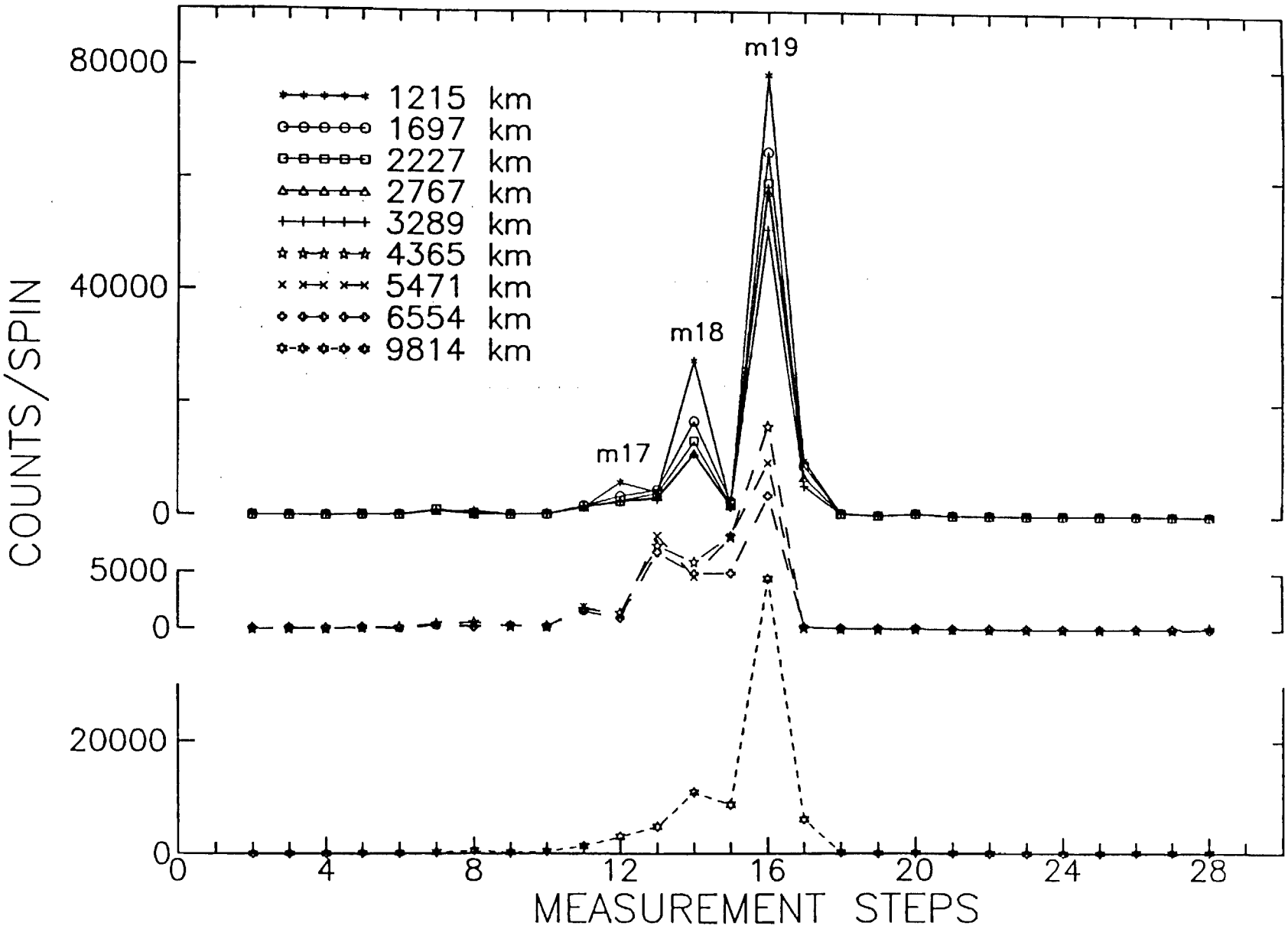
80000
40000
0
5000
0
20000
0
0
4
8
12
16
20
24
28
COUNTS/SPIN
MEASUREMENT STEPS
m17
m18
m19
1215 km
1697 km
2227 km
2767 km
3289 km
4365 km
5471 km
6554 km
9814 km

Fig. 1

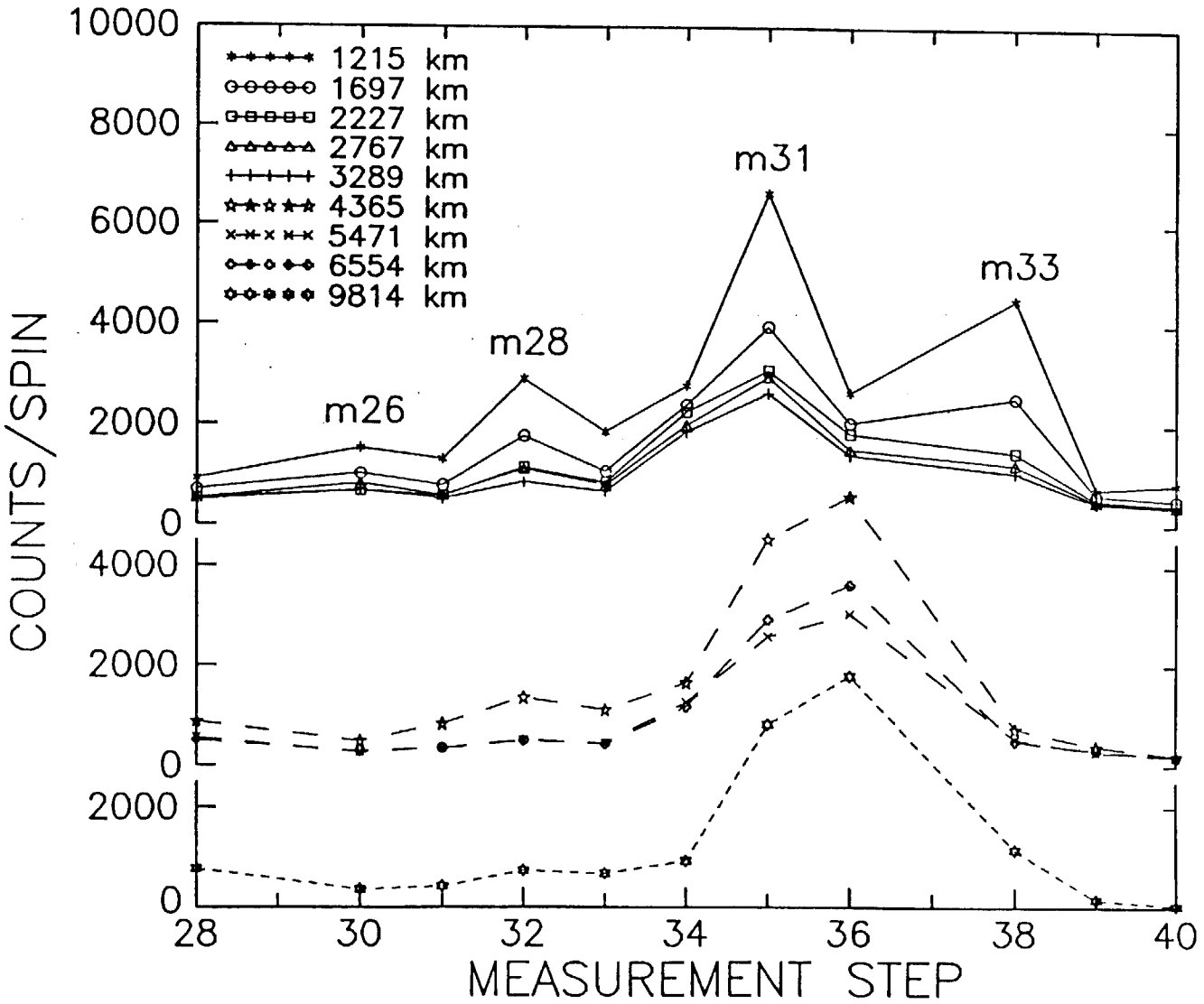
10000
8000
6000
4000
2000
0
4000
2000
0
2000
0
COUNTS/SPIN
1215 km
1697 km
2227 km
2767 km
3289 km
4365 km
5471 km
6554 km
9814 km
m26
m28
m31
m33
28
30
32
34
36
38
40
MEASUREMENT STEP

Fig. 2

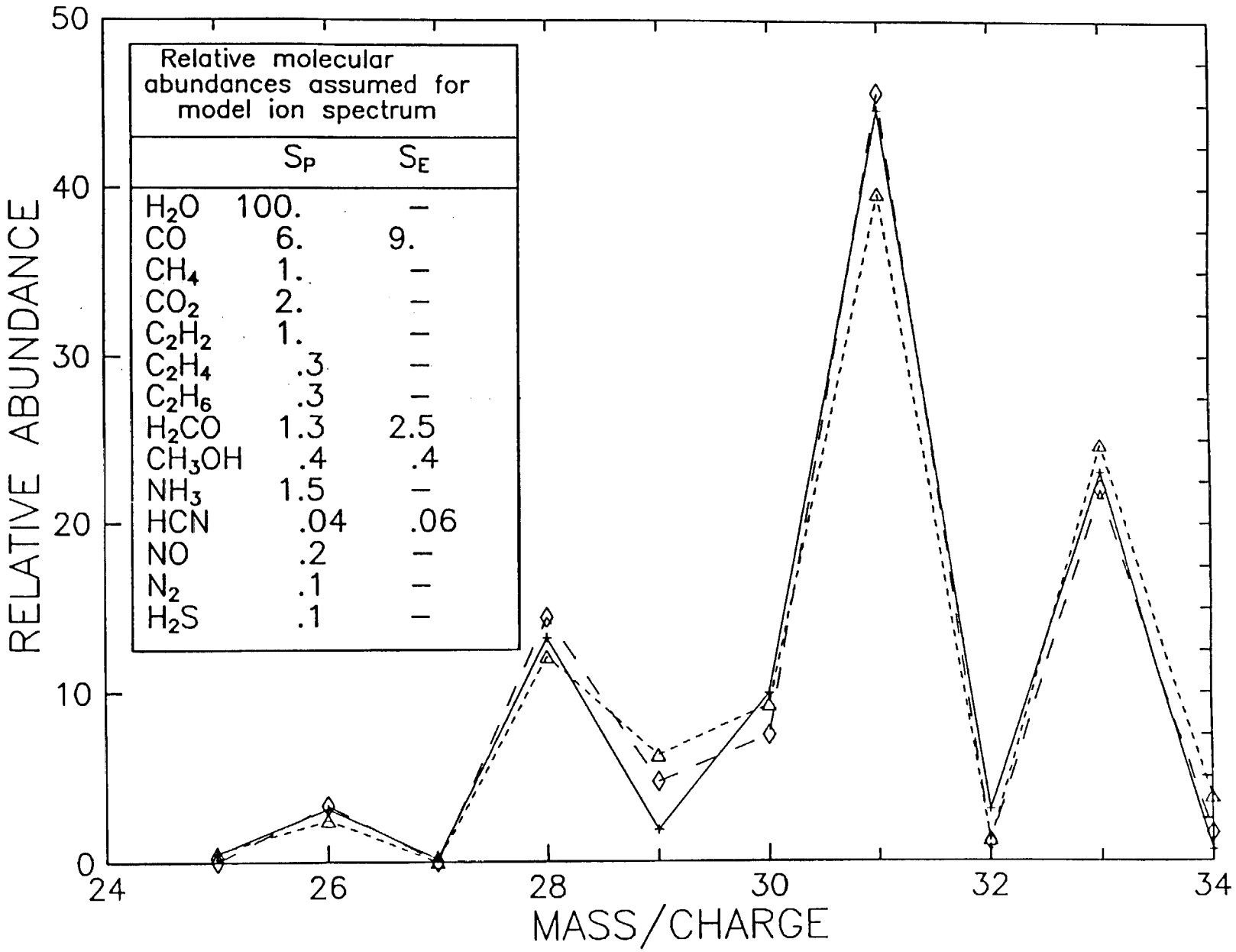
Relative molecular abundances assumed for model ion spectrum
S_P S_E
H_2O 100. –
CO 6. 9.
CH_4 1. –
CO_2 2. –
C_2H_2 1. –
C_2H_4 .3 –
C_2H_6 .3 –
H_2CO 1.3 2.5
CH_3OH .4 .4
NH_3 1.5 –
HCN .04 .06
NO .2 –
N_2 .1 –
H_2S .1 –
RELATIVE ABUNDANCE
0
10
20
30
40
50
24
26
28
30
32
34
MASS/CHARGE

Fig. 3